Hanh Bui, Mauricio Reyes Canales, Javad Yusifbayov, Tyler Hauck, and Chet Goerzen

Alberta Geological Survey
Suite 205, Twin Atria Building
4999-98 Avenue
Edmonton, AB
ags.aer.ca

High-resolution nodal seismic catalogs for improved subsurface interpretation in the Peace River region, Northwestern Alberta

Abstract

Seismic nodal arrays are increasingly used in local-scale seismic studies due to their rapid deployment, cost-effectiveness, and ability to provide high resolution event locations that enhance the characterization of seismic clusters. The Reno seismic nodal array was rapidly deployed following the November 29, 2022 seismic event with a local magnitude (ML) of 5.59 in the Reno area, Peace River region, to record the associated aftershock sequence. This dataset, previously analyzed in earlier studies, offers valuable insight into event distributions and source characteristics. In this work, we reprocess the same dataset across three deployment rounds and detect nearly 3,300 seismic events, including more than 2,200 events from the first round, 150 events from the second round, and nearly 900 from the third round. The resulting high resolution locations show that most events occur between 2 and 6 km below the ground surface, indicating seismicity primarily within the Precambrian basement. Two main seismic sub-clusters are identified in the vicinity of two disposal wells, demonstrating the improved local resolution provided by the nodal array, which is critical for assessing potential induced seismicity. The rapid response deployment enhanced detection of smaller-magnitude events, improved local data quality, and enabled more reliable magnitude estimates. This resulted in a more complete seismic catalog, better-resolved event locations, and improved characterization of seismicity. Overall, the enhanced dataset contributes to a better understanding of the spatiotemporal evolution of seismicity in the region and its induced origin related to disposal activities in the Leduc Formation.

Introduction

In late November 2022, an ML 5.59 mainshock occurred in the Reno area, about 38 km southeast of Peace River, marking one of the largest instrumentally recorded earthquakes in Alberta. At the time, the Regional Alberta Observatory for Earthquake Studies Network (RAVEN) provided limited coverage near the epicentre, restricting detection of small aftershocks and resulting in relatively high location uncertainties (Gu et al., 2025). To address this, the Alberta Geological Survey and the University of Alberta deployed a rapid-response nodal array in the Reno area in three data-gathering rounds between December 6, 2022, and April 15, 2023, to capture the evolving aftershock sequence.

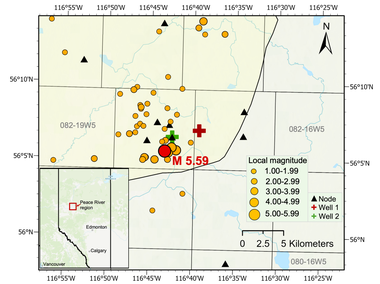

Figure 1. Regional-array seismicity with two nearby disposal wells: Well 1 injects into the Leduc Fm. (~2 km depth) and Well 2 into the Belloy Fm. (~0.7 km depth).

Data from these deployments have been analyzed in several studies (Li et al., 2023; Vasyura Bathke et al., 2023; Salvage et al., 2024; Gu et al., 2025; Sun et al., 2026; Reyes Canales et al., 2026). Machine-learning-based processing of the first deployment round identified over 1,000 aftershocks and revealed fault lineaments previously undetected by the regional network (Li et al., 2023). An analysis using the entire deployment period detected over 2,000 events, demonstrating the effectiveness of a dense local network in this limited station coverage region (Gu et al., 2025). Subsequent work identified a total of 2,213 events across the three rounds (with 1,586 events from the first round alone), further highlighting the value of high-density nodal arrays for resolving aftershock distributions and imaging basement faulting (Sun et al., 2026).

The Reno nodal dataset contains crucial information for interpreting subsurface structure, seismic clustering, and induced fault reactivation processes. To fully leverage its high resolution, each of the three deployment rounds was reprocessed independently using a comprehensive workflow designed for nodal array data, and all detected events were carefully reviewed to improve location accuracy and magnitude estimates.

Data and Methods

Data Overview

The dataset comprises 205 gigabytes of three-component continuous seismic recordings collected over three deployment rounds: 9 nodes in Round 1, 6 nodes in Round 2, and 7 nodes in Round 3. Overall, the data quality is quite high, with data continuously recorded across all deployments.

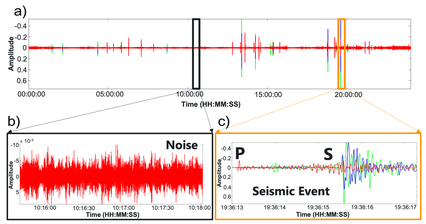

Figure 2. Example of (a) one day of three-component nodal array data, (b) a noise segment, and (c) a seismic event (vertical component: red; horizontal components: blue and green).

Processing Workflow

We processed three rounds of seismic data using a consistent workflow.

Preprocessing of nodal data is a critical step that facilitates subsequent analyses. It includes data conversion, detrending, and noise filtering.

We applied a recursive STA/LTA algorithm (Withers et al., 1998; Trnkoczy, 1999) with a low detection threshold to capture almost all seismic events. To be classified as a true event, the signal had to be recorded by at least three seismic nodes; detections observed on only one or two nodes were discarded as noise.

P- and S-wave arrivals were picked and manually reviewed to ensure timing accuracy.

Hypocenter locations were determined using NonLinLoc with the oct-tree importance sampling algorithm (Lomax et al., 2000, 2014). This method accelerates grid searches by recursively subdividing high-probability cells, producing a location probability density function, with the optimal hypocenter corresponding to the minimum misfit point.

The events were then relocated using HypoDD (Waldhauser, 2001) to further improve relative location accuracy.

Local magnitudes were calculated using Yenier's (2017) regionally calibrated formula for the Western Canada Sedimentary Basin (WCSB).

This workflow resulted in a final event catalog that includes the origin time, hypocenter location, and magnitude for each event.

Note: For event location, we used a one-dimensional (1D) velocity model for the Peace River region derived from P-wave sonic logs of nearby wells.

Event Detection Results

Figure 4 shows the event detection results for the three rounds of data. Round 1 recorded the largest number of events, with high daily counts because the array was deployed immediately after the mainshock ML = 5.59, followed by a steady decrease in seismicity reflecting the expected aftershock decay pattern; Round 3 recorded the next highest number of events, beginning with a few detections, then exhibiting increasing activity associated with the ML = 5.09 event in March 2023 and subsequently decreasing as its aftershocks diminished and Round 2 recorded the fewest events, with only a small number detected each day.

Table 1. Comparison of detected seismic events from three rounds of the Reno seismic nodal array. Abbreviations: R1, Round 1; R2, Round 2; R3, Round 3; NA, Not analyzed.

Data	Events detected by this study	Events detected by Sun et al., (2026)	Events missed by Sun et al., (2026)	Events detected by Li et al., (2023)	Events missed by Li et al., (2023)
R1	2239 events	1586 events	653 events	1241 events	998 events
R2	150 events	128 events	37 events	NA	
R3	870 events	499 events	371 events	NA	

Event Location Results

Figure 5 shows the relocated event locations from three rounds of data. Two seismic sub-clusters are observed near two disposal wells in both map view and depth views. Most events occur between 2 and 6 km depth, with the upper portion of the cluster reaching the top of the basement at approximately 2 km. These high resolution event locations are crucial for understanding the induced origin of the seismicity associated with disposal activities into the Leduc Formation and potential basement rooted faults, resulting in earthquakes that occur deeper than the target injection interval.

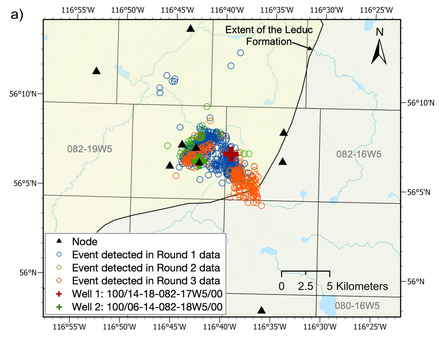

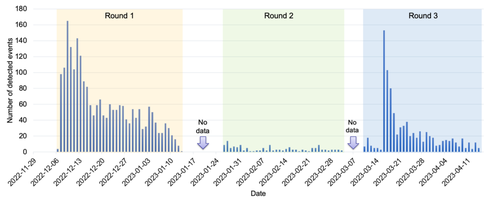

Figure 4. Events identified from three rounds of data by using the STA/LTA method.

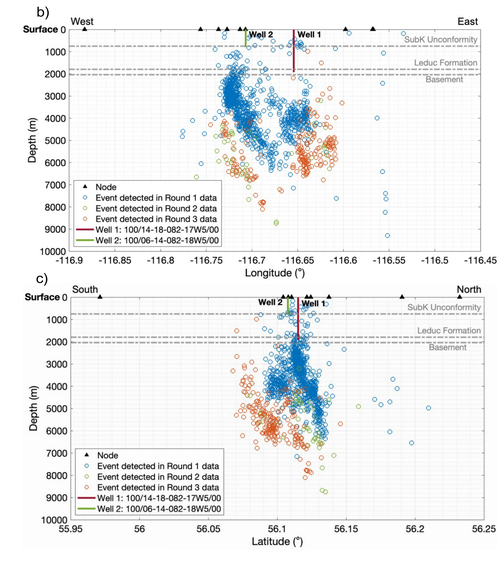

Figure 5. (a) Map view and (b), (c) depth views of events detected by the nodal array detected from Round 1 (open blue circles), Round 2 (open green circles), Round 3 (open orange circles), plotted together with the node locations (black triangles), formation boundaries, and disposal well locations. .

Magnitude Estimation

Local magnitudes were calculated using the Yenier (2017) formula. Figure 6 shows the histogram of estimated local magnitudes for all detected events. The magnitude of completeness (Mc), estimated using the maximum curvature method (Wiemer and Wyss, 1997), is approximately -0.42, indicating that all events above this Mc value are considered to be reliably detected and recorded.

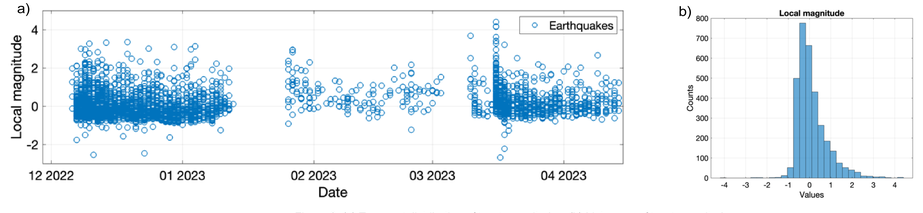

Figure 6. (a) Temporal distribution of local magnitudes, (b) histogram of local magnitudes.

Discussion

Waveform Clipping Effect

Round 3 includes one of the largest events in the sequence, the ML = 5.09 earthquake in March 2023. However, because of waveform clipping effects, where signal amplitudes exceed the upper limit of the instrument's dynamic range, the recorded data became saturated, causing the calculated local magnitude of this event to be underestimated at 4.40. Clipped waveforms cannot be used reliably for magnitude estimation, and this limitation affects larger magnitude events.

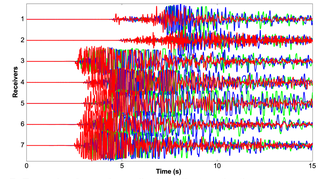

Figure 7. Example of waveform clipping effect on the three-component data (vertical component: red; horizontal components: blue and green).

Conclusions

This study provides a high resolution seismic event catalog derived from three rounds of nodal array deployment, demonstrating the capability of nodal arrays to enhance local scale seismic monitoring. Reprocessing the full dataset identified nearly 3,300 seismic events, with Round 1 recording the highest number of events, followed by Round 3 and Round 2. Event locations reveal two seismic sub-clusters situated near two disposal wells, with most events occurring between 2 and 6 km depth within the Precambrian basement. The refined locations, together with local magnitude estimates, result in a more complete and reliable catalog that better resolves event distributions and underlying structural patterns. These enhanced observations improve resolution of the spatiotemporal evolution of seismicity in the Reno area and provide stronger constraints on its induced origin related to disposal activities in the Leduc Formation.

Acknowledgements

The authors would like to thank Shaurat Sayani, Nick Roman, Jason Hendrick, Alex MacNeil, Todd Shipman, Chris Filewich, Kelsey MacCormack, and Andrew Beaton (Alberta Geological Survey and Alberta Energy Regulator) for their constructive and helpful support developing this project.

References

Gu, Y. J., W. Sun, T. C. Yu, J. Wang, R. Wang, T. Li, and R. Schultz, 2025, Peace River Induced Seismic Monitoring (PRISM) Nodal Seismic Array: Seismological Research Letters, 96(1), 562–575.

Li, J., J. Rojas Parra, R. O. Salvage, D. W. Eaton, K. A. Innanen, Y. J. Gu, and W. Sun, 2024, Machine learning aids rapid assessment of aftershocks: Application to the 2022–2023 Peace River earthquake sequence, Alberta, Canada: The Seismic Record, 4(1), 21–31.

Lomax, A., J. Virieux, P. Volant, and C. Berge Thierry, 2000, Probabilistic earthquake location in 3D and layered models: Introduction of a Metropolis–Gibbs method and comparison with linear locations: In C. H. Thurber and N. Rabinowitz (eds.),Advances in Seismic Event Location, Modern Approaches in Geophysics, vol. 18, Springer, Dordrecht, Netherlands, 101–134.

Lomax, A., A. Michelini, and A. Curtis, 2014, Earthquake location, direct, global-search methods: In R. A. Meyers (ed.), Encyclopedia of Complexity and Systems Science, Springer, New York, 1–33.

Mei, S., 2009, New insights on faults in the Peace River Arch region, northwest Alberta, based on existing well log data and refined trend surface analysis: Canadian Journal of Earth Sciences, 46(1), 41–65.

O'Connell, S. C., G. R. Dix, and J. E. Barclay, 1990, The origin, history, and regional structural development of the Peace River Arch, Western Canada: Bulletin of Canadian Petroleum Geology, 38A, 4–24.

Reyes Canales, M., T. Hauck, J. A. Yusifbayov, H. Bui, and C. Goerzen, 2026, Discerning between natural and induced seismicity by using evidence-scoring tools designed to evaluate proposals of induced earthquakes: Application to the Reno and Kakwa earthquake clusters: Alberta Energy Regulator / Alberta Geological Survey, AER/AGS Open File Report 8445, 29 p.

Salvage, R. O., D. W. Eaton, C. M. Furlong, J. Dettmer, and P. K. Pedersen, 2024, Induced or natural? Toward rapid expert assessment, with application to the Mw 5.2 Peace River earthquake sequence: SRL, 95(2A), 758–772

Sun, W., Y. J. Gu, Y. Liu, T. Li, R. Wang, J. Wang, R. Harrington, M. Roth, R. Schultz, G. Xu, and G. Jiang, 2026, Rupture cascade initiated by wastewater disposal: Nucleation and domino effect of Canada's largest induced earthquake: Geophysical Research Letters, 53(1), e2025GL118405.

Trnkoczy, A., 1999, Understanding and parameter setting of STA/LTA trigger algorithm: In P. Bormann (ed.), New Manual of Seismological Observatory Practice 2 (NMSOP-2), Deutsches GeoForschungsZentrum GFZ, Potsdam, Germany, 1–20.

Vasyura Bathke, H., J. Dettmer, K. Biegel, R. O. Salvage, D. Eaton, N. Ackerley, S. Samsonov, and T. Dahm, 2023, Bayesian inference elucidates fault-system anatomy and resurgent earthquakes induced by continuing saltwater disposal: Nature Communications Earth & Environment, 4, 407, doi:10.1038/s43247-023-01064-1.

Waldhauser, F., 2001, HypoDD – A program to compute double difference hypocenter locations: U.S. G. S, Open File Report 2001 113.

Wiemer, S., and M. Wyss, 1997, Mapping the frequency–magnitude distribution in asperities: An improved technique to calculate recurrence times?: Journal of Geophysical Research: Solid Earth, 102, 15115–15128.

Withers, M., R. Aster, C. Young, J. Beiriger, M. Harris, S. Moore, and J. Trujillo, 1998, A comparison of select trigger algorithms for automated global seismic phase and event detection: Bulletin of the Seismological Society of America, 88(1), 95–106.

Yenier, E., 2017, A local magnitude relation for earthquakes in the Western Canada Sedimentary Basin: Bulletin of the Seismological Society of America, 107(3), 1421–1431.